Materials Chemistry and Physics 115 (2009) 551–556

Contents lists available at ScienceDirect

Materials Chemistry and Physics

journal homepage: www.elsevier.com/locate/matchemphys

# Surface roughening and transport properties in the growth of nano-structured nickel electrodeposits on ITO substrate

L. Nzoghe-Mendome[a], A. Aloufy[c], J. Ebothé[a,*], D. Hui[b], M. El Messiry[c]

[a] Laboratoire de Microscopies & d'Etude de Nanostructures, E.A. n°3799, UFR Sciences, Université de Reims, B.P. 138, 21 rue Clément Ader, 51685 Reims Cedex 02, France
[b] University of New Orleans, Dept of Mechanical Engineering, New Orleans, LA 70148, USA
[c] Alexandria University, New Advanced Materials & Nanotechnology Center, Faculty of Engineering Textile & Material, Engineering Department, 21544 Alexandria, Egypt

ARTICLE INFO

*Article history:*
Received 12 September 2008
Received in revised form
10 November 2008
Accepted 13 December 2008

*Keywords:*
Metals
Surfaces
Thin films
Atomic force microscopy (AFM)
Electrochemical technique

ABSTRACT

We here show that indium tin oxide (ITO)-coated glass can be an interesting substrate for the electrodeposition of separated nickel crystallites growing in the face-centred cubic (fcc) structure. The resulting bi-modal film surface morphology corresponds to the formation of vertical crystallites whose size can reach 400 nm mean height. The topography study confirms the occurrence of both the lateral and vertical growth orientations as the growth exponent coefficient always remains $\beta > 0.50$, which is characteristic of such an effect. We also show that the model of link between the topography and surface transport properties is relevant here, which gives it a more general validity. The surface diffusion of the Ni ad-atoms on ITO range in the interval $10^{-10} < D_s < 10^{-9}$ cm$^2$ s$^{-1}$ that is higher than the values obtained on metal substrates. The increase of $J$ favours the vertical growth as the surface diffusion length, $\Lambda_s$, decreases with the increase of the crystallites size.



## 1. Introduction

The growth process and its related mechanisms remain so far the first concern of investigations on the materials formation. In the last decades, a real effort in this direction has been done for nano-dots and nano-wires whose properties markedly deviate from those of bulky coalesced samples due to the size reduction and confinement effects [1–3]. In that frame of nano-science and nano-technology, materials in the form of nano-structured films are not sufficiently explored till now. They offer the advantage of a better experimental access due to the required deposition surface. As well admitted now, their mesoscopic thickness scale of less than 1 μm enhances the role of surface irregularities limited to 100 nm mean square roughness on their properties [4]. Consequently, the strong relation between the growth process and the film surface feature appears as a necessary objective to be established in that case. By and large, both aspects are seldom correlated as the usual approaches to the film's surface features are mostly static and descriptive. In electrodeposition, the diffusion of the involved ion species in the electrolyte is known to affect the morphological stability of a nascent film [5]. However, the dependence of the film morphology on the material surface transport properties is mentioned only in very limited reports. Modelling the surface diffusion of metallic ad-atoms at electrochemical interfaces has been proposed by Alonso et al. [6] for the case of gold and platinum films using observations obtained from electron microscopy studies. This model has been adapted by Hiane and Ebothé [7] in the electrodeposition of Ni–Zn alloys on copper substrate for the evaluation of the material composition effects. A direct link between the material surface transport properties and the sample topography parameters has been examined for that case. However, several deposition parameters can affect the material transport properties and the resulting surface morphology of nano-structured films. The present work confirms the fact that the model proposed with alloys can be also valid for pure metal electrodeposits and then used in a more general way under specific conditions. The study is here undertaken with nickel nano-structured films deposited on indium tin oxide (ITO) substrate. Actually, nickel is widely used in a large number of application fields and mostly as a component of some specific devices [8–10]. Saitou et al. [11,12] and also Gomez et al. [13] showed that ITO can be a relevant substrate for Ni films as it appears for many materials involved in electronic and opto-electronic areas due to its excellent transparent and highly conductive characteristics. Moreover, it is known to be non-sensitive to external air and humidity, which makes it a very suitable substrate in various experimental environments. Therefore, understanding the surface feature formation of nickel nano-structured films on such kind of substrate materials can be of real interest. The outline of this work consists in Section 2 of experimental part including the film preparation procedure and the presentation of the different techniques and conditions

* Corresponding author. Tel.: +33 3 26 05 19 01; fax: +33 3 26 05 19 00.
*E-mail address:* jean.ebothe@uni-reims.fr (J. Ebothé).

0254-0584/$ – see front matter © 2009 Published by Elsevier B.V.
doi:10.1016/j.matchemphys.2008.12.014

used for the material characterisation. The obtained results and the engendered discussion are proposed in Section 3 where the relationship between the surface diffusion and topography of the nano-structured nickel films are analysed.

## 2. Experimental

### 2.1. Deposition procedure of Ni electrodeposits

Ni electrodeposits are prepared in a three-electrode cell system from a 1-M $Ni(SO_4)_2$ aqueous electrolyte made of a FLUKA product (purity > 99%). Its pH ≈ 3.5 is maintained by adding boric acid (0.3 M) in the medium. A stationary substrate of 0.5 $cm^2$ area is used as working electrode made of (ITO)-coated glasses of DIAMOND COATINGS LIMITED company whose sheet resistivity is evaluated at 20 Ω $sq^{-1}$. This value reflects a sufficient electrical conductivity of this material for this particular role. A platinum sheet counter electrode of the same area faces the working one 2.5 cm away while a saturated calomel electrode (SCE) serves for the potential reference. This cell is kept in a constant temperature $T$ = 323 K without stirring. The electrochemical experiments are performed from a radiometer PGP 201 galvanostat/potentiostat, the films being deposited in a constant current mode using the chrono-amperometry technique. The investigated current densities are ranged between 10 and 25 mA $cm^{-2}$ and the deposition time is adjusted in every case for having a final film thickness $d \approx 1$ μm. These conditions have been found suitable for the topography limitations of nano-structured films as defined above. Moreover, 1 μm thickness of the Ni films can be considered as safe for any substrate topography disturbance since the ITO surface irregularities were measured as having about 3 nm root-mean-square (rms) roughness.

### 2.2. Experimental techniques

Once formed, the thickness of the Ni electrodeposits is measured by a commercial STRATAGem (SAMx, France) software associated with the X-ray microanalysis, the related spectra being acquired at about 25 kV in a collecting time of 100 s, as described in Refs. [14,15]. Accordingly, the thickness value is referred to the X-ray intensity of the substrate material elements. The film's structure is analysed from a BRUCKER D8 ADVANCED X-ray apparatus with a Cu (Kα) irradiation λ = 1.540 Å. Their nano-scaled topography is examined by atomic force microscopy (AFM) with a stand-alone SMENA set-up operating in a constant contact force mode. The collection of AFM images and the measurement of the inherent topography parameters are performed in ambient atmosphere. Every image is digitised into (512 × 512) pixels with a scanning frequency of about 1 Hz. The cantilever is composed of a commercial $Si_3N_4$ tip of approximately 20 nm apex radius bearing a 0.06 N $m^{-1}$ spring coefficient. To avoid tricky results, as it may be induced by the tip effect, and then be ensured on the imaging process, several new tips are used to analyse the same sample area. Besides, the local topography parameters are measured from nearly 15 zones of the same film surface, the statistical accuracy being improved by repeating the same procedure to 10 samples deposited under strictly the same conditions. These parameters are hereby supplied with a relative uncertainty less than 10%.

## 3. Results and discussion

### 3.1. Structure and morphology of the investigated Ni samples

Although the investigated Ni samples have been deposited at different growth rates, we did not notice a real change on the X-ray diffraction patterns of the samples. This could be ascribed to the relative narrow region of the applied current densities. In every case, the different peaks labelled in Fig. 1 are the lines of face-centred cubic (fcc) structure of Ni with a cell parameter of $a$ = 3.52 Å. According to the order of the peak's intensities obtained, the predominance of (1 1 1) line is here clearly depicted that is subsequently followed by those of the (2 0 0), (2 2 0) and (3 1 1) lines. The study of the sample's surface feature from the AFM–3D images of Fig. 2 shows that Ni films grow with the formation of separated nano-crystallites evolved all over the film surface. The comparison of the images of Fig. 2(a–c) denotes an increase of their size with $J$ value although their shape remains the same. These images show that the increase of $J$ also leads to the increasing of the nano-crystallites density. This surface feature evolution implies that the growth process mostly occurs at particular nucleation sites where these nano-crystallites are preferentially formed, the coalescing area being relatively large. As known in that case, the growth process is influenced by the specific properties of the film–substrate interface such as the free surface energy of both materials, the adhesion energy and the crystallographic mismatch at the nucleus–substrate boundary. Since our ITO is quite amorphous, it can be expected that the interface energy aspects prevail on the crystallographic ones. However, more experiments are needed for an effective evaluation of these effects.

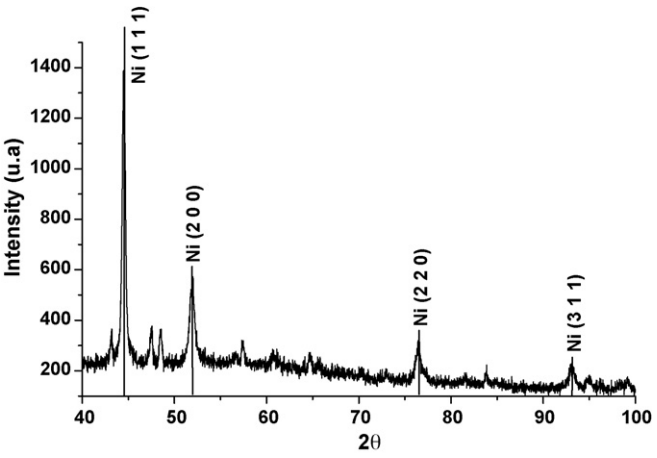


**Fig. 1.** X-ray diffraction of nano-structured Ni electrodeposits of 1 μm thickness in the range of the investigated growth rates.

The surface morphology histogram of the Ni films related to the AFM images, modelled in Fig. 3. By successive Gaussian curves, confirms the evolution of the film morphology due to the applied current density. The results obtained at higher $J$ values clearly reveal in Fig. 3(b) and (c) that the film growth practically proceeds from a bi-modal process characterized by a background of predominant small grains (smaller heights, $h_o$) whose size contrasts to the one of the bigger nano-crystallites (higher heights, $h'$). The Gaussian maximum depicting the average grain height, the results proposed in Table 1 show that the increase of $J$ linked to the one of the film thickness leads to a shift of $h_o$ and $h'$ towards higher values. However, it appears that $h'$ is more sensitive to the $J$ effect while the difference between $h_o$ and $h'$ neatly collapses at lower $J$ values. This specific morphology seems quite different from those obtained by Saitou et al. [11,12] on the same substrate material. This could be ascribed to the relative high range of the $J$ values used and probably also to the ITO resistivity as underlined elsewhere [16]. The results proposed here could be interesting in many application fields. A local study for instance can lead to determine the size limit for which the nano-crystallites obtained can exhibit either a mono-domain or a multi-domains magnetic configuration. Besides, the limit of confinement effects can also be investigated this way. For larger surface scales, the resulting grain features seem quite adapted for tribology and adherence applications.

### 3.2. Topography study of the Ni nano-structured films

The evolution of the film surface morphology as shown above promotes to study the dependence of the film's topography parameters on $J$ value. As mentioned above, the Family–Vicsek approach

**Table 1**
Dependence of the average grain and nano-crystallite heights and film thickness on the current density parameter for the Ni samples obtained at the common deposition time $t$ = 60 s.

| Current density $J$ (mA $cm^{-2}$) | Small grains height $h_o$ (nm) | Crystallites height $h'$ (nm) | Film thickness $d$ (μm) |
|---|---|---|---|
| 10 | 121 ± 0.2 | 121 ± 0.3 | 0.22 |
| 14 | 213 ± 0.1 | 213 ± 0.1 | 0.320 |
| 18 | 254 ± 0.3 | 290 ± 0.2 | 0.380 |
| 22 | 335 ± 0.2 | 400 ± 0.1 | 0.422 |

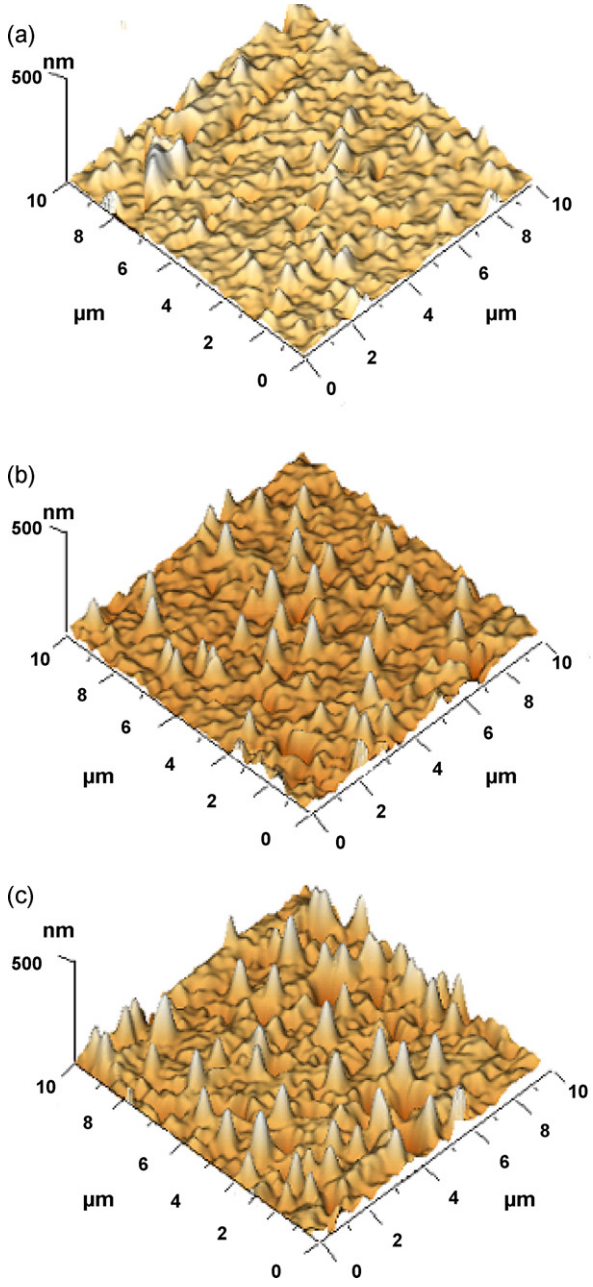


**Fig. 2.** AFM–3D images of nano-structured Ni electrodeposits of 1 μm thickness obtained at different growth rate values: (a) $J = 16\ \mathrm{mA\,cm^{-2}}$; (b) $J = 18\ \mathrm{mA\,cm^{-2}}$; (c) $J = 20\ \mathrm{mA\,cm^{-2}}$.

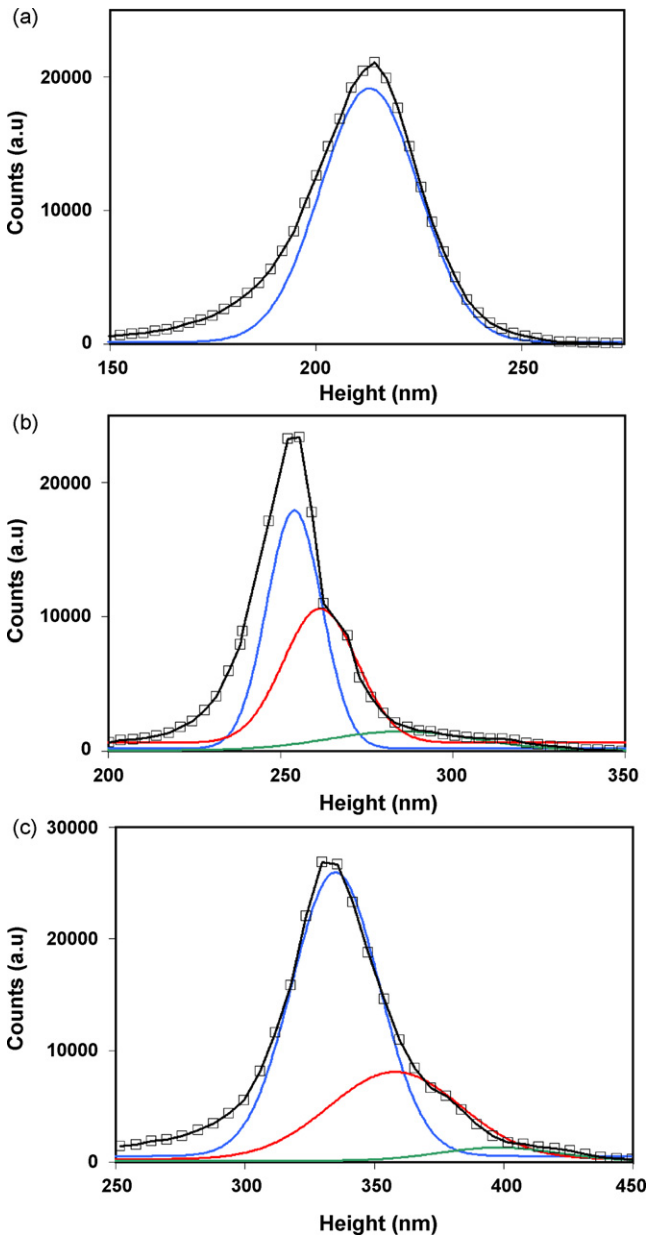


**Fig. 3.** Surface morphology histograms as modelled by the Gaussian fit for three samples obtained at different growth rate values: (a) $J = 14\ \mathrm{mA\,cm^{-2}}$; (b) $J = 18\ \mathrm{mA\,cm^{-2}}$; (c) $J = 22\ \mathrm{mA\,cm^{-2}}$.

[17,18] based on the scaling behaviour of the interface width or local root-mean-square surface roughness ($\sigma$) is suitable in the present case as it has been shown previously [19,20]. The method applied is here undertaken according to the roughness expression

$$\sigma(L) = \frac{1}{N(L)} \left\{ \sum_{n=1}^{N} \sum_{m=1}^{N} [h(x_n, y_m) - \hbar]^2 \right\}^{1/2} \quad (1)$$

where $h(x, y)$ is the height at a pixel of the analysed area; $N$, the total number of pixels in this area; $\hbar$, the related average height value and $L$, the linear length or scale of the analysed area. This spatial analysis corresponds to the predicted conditions:

$$\sigma(L) \propto L^{\alpha} \quad \text{for } L \ll Lc \quad (2)$$

$\alpha$, is another topography parameter named roughness exponent. The asymptotic onset of the $\sigma(L)$ dependence corresponds to two main topography parameters, $\sigma_{sat}$ and $Lc$, both linked to the deposition conditions of the investigated film. $\sigma_{sat}$ also named global roughness, gives a vertical feature of the nano-scaled surface irregularities while $Lc$ depicts the horizontal one. The dynamic analysis of the film formation is referred to the predicted condition

$$\sigma_{sat}(t) \approx t^{\beta} \quad \text{for } L \gg Lc \quad (3)$$

with $t$ the film deposition time and $\beta$ the growth exponent. The knowledge of both $\alpha$ and $\beta$ lead to the identification of the growth mode evolved [21].

Fig. 4 depicts the general scaling profile of the film's surface roughness obtained in the range of the investigated current values as illustrated for the cases of $J = 10$ and $18\ \mathrm{mA\,cm^{-2}}$. This profile is characterised by two different linear zones of $\alpha_1$ and $\alpha_2$ slopes respectively preceding the saturation onset of the $\sigma = f(L)$ curves.

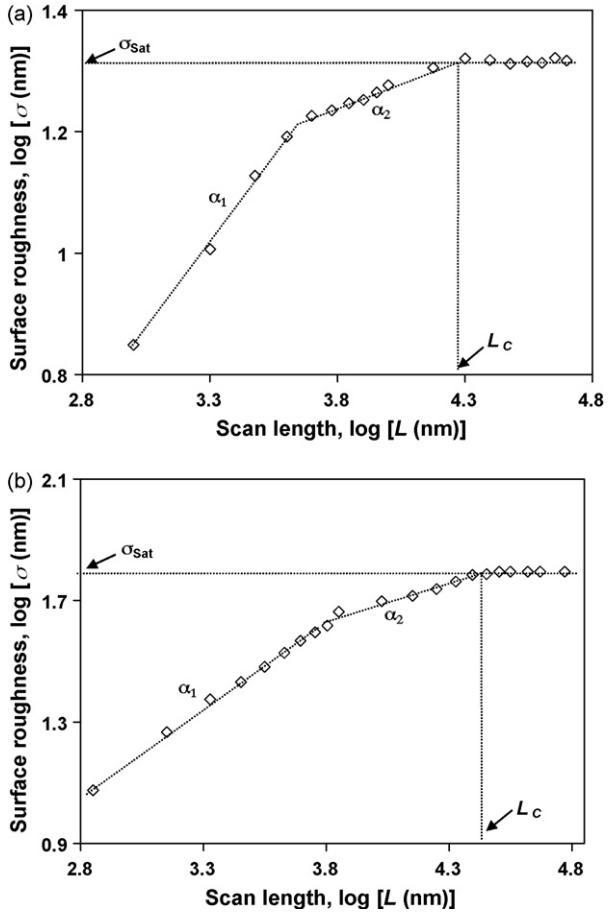


**Fig. 4.** Scaling feature of the surface roughness for the samples formed at two different growth rates: (a) $J = 10\,mA\,cm^{-2}$ and (b) $J = 22\,mA\,cm^{-2}$.

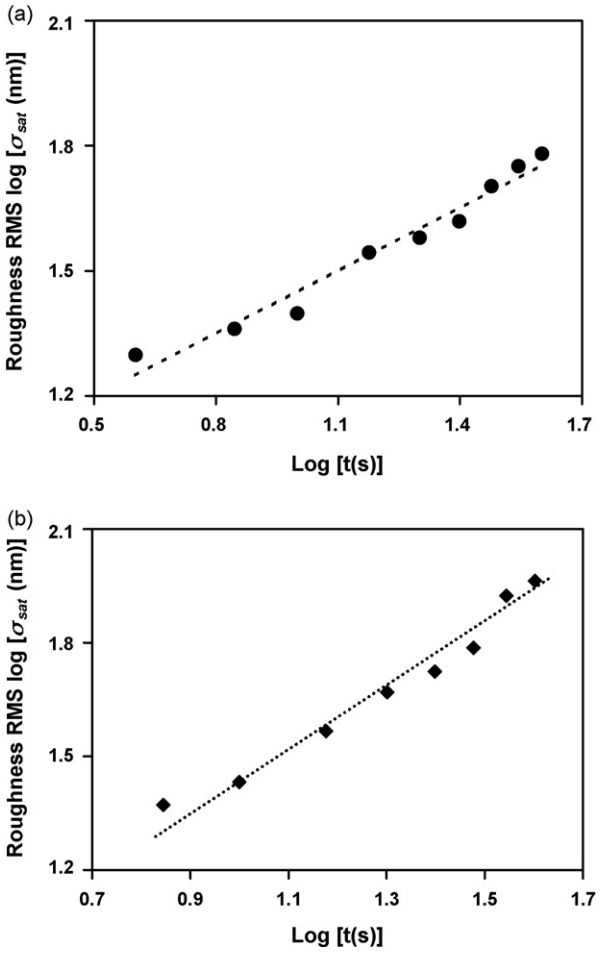


**Fig. 5.** Scaling feature of the saturated surface roughness with the film deposition time for the two extreme growth rate values: (a) $J = 10\,mA\,cm^{-2}$ and (b) $J = 22\,mA\,cm^{-2}$.

All the results proposed in Table 2 show that the two slopes are ranged in the intervals $0.50 < \alpha_1 < 0.65$ and $0.10 < \alpha_2 < 0.20$. This curve profile deviates from the theoretical prediction corresponding to a single linear zone. On the other hand, the logarithmic fitting in the $L$ axis used here can be considered as sufficient for experimental results in agreement with many authors as the covering of some orders in magnitude is fully possible only for the computer-simulated analyses [19]. Experimentally, such double scaling linearity was already reported for some metal alloys grown on metallic substrates [19,20] and also for pure metals on specific substrates as glassy carbon [22,23]. Although this result has a link with the deposition conditions, no clear explanation does exist for that so far. Recently, Oliviera and Aarao Reis [24] proposed a model for which the range of $\alpha_1$ and $\alpha_2$ values is associated with the shape and size distribution of the grains. In actual fact, the values $0.10 < \alpha_2 < 0.20$ of Table 2 are nearly in agreement with the smoothest background surface features having large cliffs described by these authors. However, the deviation of our $\alpha_1$ from their interval $0.85 \leq \alpha_1 \leq 1$ implies that our results does not match with their updated Kardar–Parisi–Zhang (KPZ) interpretation of the growth mode. The dynamic study based on the evolution of the global roughness always leads to a single sloped linearity of the $\sigma_{sat} = f(t)$ curve as illustrated in Fig. 5. The dependence of the resulting growth exponent $\beta$ on $J$ in Table 2 always shows that $\beta > 0.5$. This behaviour along with the predominance of the [1 1 1] growth orientation of the Ni electrodeposits concurs with the result of Saitou et al. [12] obtained at lower $J$ values. On the other hand, $\beta > 0.5$ has been interpreted as being characteristic of a difference in the atomic diffusivity between the normal and the parallel directions to the deposition substrate, whose various possible origins (Shadowing effect, Schwoebel barrier and so on) have been summarized in Refs. [19,25]. This observation promotes to examine the material transport properties in each one of the two directions as it is considered in the next section. Finally, the set of $\alpha$ and $\beta$ values obtained here are difficult to be considered in terms of growth model in the universality class as it could be expected.

The global description of the film's topography remains unsatisfactory when $\sigma_{sat}$ or $Lc$ is separately considered so far as both parameters are intimately related in the film formation. Accordingly, the topography factor defined as $k = \sigma_{sat}/Lc$ seems more

**Table 2**
Dependence of the topography parameters on the applied current density for Ni films of 1 μm thickness.

| Current density $J$ ($mA\,cm^{-2}$) | Roughness exponent 1, $\alpha_1$ | Roughness exponent 2, $\alpha_2$ | Growth exponent $\beta$ | Topography factor $k = \sigma_{sat}/Lc$ (a.u.) |
|---|---|---|---|---|
| 10 | 0.56 ± 0.02 | 0.12 ± 0.01 | 0.50 ± 0.03 | 1.54 |
| 14 | 061 ± 0.02 | 0.22 ± 0.01 | 0.71 ± 0.03 | 0.98 |
| 18 | 0.55 ± 0.01 | 0.18 ± 0.01 | 0.86 ± 0.01 | 1.20 |
| 22 | 0.71 ± 0.01 | 0.21 ± 0.01 | 0.67 ± 0.01 | 2.70 |

adapted here to evaluate the influence of the current density. One observes in Table 2 that $k$ has a minimal value 0.98 at $J = 14\ \text{mA cm}^{-2}$, which implies one has here a relative higher lateral ($Lc$) topography parameter. This is likely to be dependent on some link with the crystallites density at the film surface, but it needs more experimental confirmation. From Tables 1 and 2 one sees that the increase of $h'$ occurs along with the one of $k$ for $J > 14\ \text{mA cm}^{-2}$ while the reversal behaviour is observed between both parameters for $J < 14\ \text{mA cm}^{-2}$. These results are likely to be connected to the nano-crystallites density but further work is needed to corroborate this assumption.

### 3.3. Study of the Ni ad-atoms transport properties in the film growth process

The topography histograms of the Ni samples proposed in Fig. 3 show that the major part of the investigated films consists of the smallest grains although the global film is concerned in the study of the material transport properties on the deposition substrate. The theoretical approach used to study the evolution of the material formation requires to examine the films having a fixed thickness value. Therefore, the deposition time is adjusted to every $J$ value, as shown in Ref. [7]. The electrodeposit topography and surface transport properties are then related through the expression

$$\frac{1}{\sigma_{sat}} = \left[3\left(\frac{2\gamma a^4 D_s}{\varepsilon_T}\right)^{1/4}\left(\frac{zF\rho}{\pi Mq}\right)\right] t^{1/4} \quad (4)$$

where $\gamma$ and $\varepsilon_T$ respectively represent the interface and the thermal energies; $a$, the lattice parameter; $D_s$, the surface diffusion coefficient of the ad-atoms; $z$, the molar charge; $F$, the Faraday number; $\rho$, the material density; $M$, the molar mass; $q$, the charge density and $t$, the film deposition time. As explained elsewhere, the linearity of the equation $(1/\sigma_{sat}) = f(t^{1/4})$ is the main condition to be fulfilled for the easy access to the surface transport properties. This linearity leads to determination of the slope constant $B$ corresponding to

$$B = 3\left(\frac{2\gamma a^4 D_s}{\varepsilon_T}\right)^{1/4}\left(\frac{zF\rho}{\pi Mq}\right) \quad (5)$$

from which is extracted the expression of the surface diffusion coefficient of the ad-atoms

$$D_s = \frac{\varepsilon_T}{2\gamma a^4}\left(\frac{B\pi Mq}{3z\rho F}\right)^4 \quad (6)$$

the diffusion length, $\Lambda_s$, being deduced from $D_s$ by the Einstein relation expressed as

$$\Lambda_s = (D_s \cdot t)^{1/2} \quad (7)$$

The plotting of the Eq. (7) have been experimentally performed here with the Ni characteristics knowing that $M(\text{Ni}) = 58.71\ \text{g mol}^{-1}$; $\rho(\text{Ni}) = 8.30\ \text{g cm}^{-3}$; $a(\text{Ni}) = 3.524 \times 10^{-8}$ cm; $\varepsilon_T(\text{Ni}) = 4.14 \times 10^{-13}$ erg at the deposition temperature $T = 323$ K; $\gamma(\text{Ni}) = 1700\ \text{erg cm}^{-2}$. The number of electrons transferred per Ni mole is $z = 2$ here with $q = 0.05\ \text{C cm}^{-2}$ and $F = 96{,}500\ \text{C mol}^{-1}$.

It comes out of the study that the link of the Ni film's $\sigma_{sat}$ with the ad-atoms transport properties of Eq. (4) is here also experimentally established. The occurrence of linearity in the plotting of the $(1/\sigma_{sat}) = f(t^{1/4})$ curves as reported in Fig. 6 confirms the validity of the model used that is observed for the film deposition time $t > 10$ s with all the investigated samples. It should be pointed out that the width of the linear zone depends on the region of $J$ value and also $d$ or $t$, one of them being constant. Experimentally, Nzoghe-Mendome [26] showed that the linearity of the $(1/\sigma_{sat}) = f(t^{1/4})$ relation always occurs in a particular time interval preceding a plateau. The results in Table 3 show that the surface diffusion of the Ni ad-atoms on ITO substrate lies from $10^{-10} < D_s < 10^{-9}\ \text{cm}^2\ \text{s}^{-1}$, which are in the range

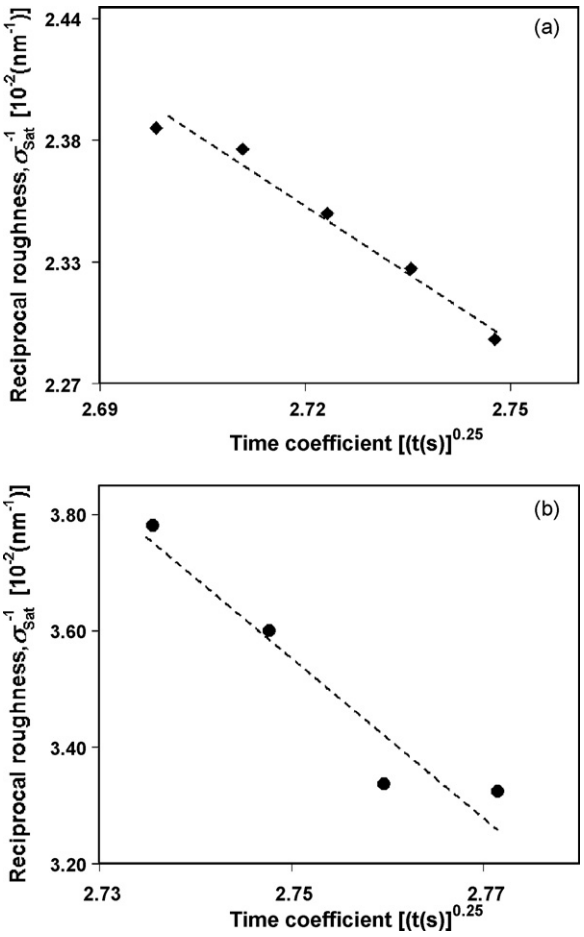


**Fig. 6.** Determination of the $B$ constant for the estimate of the Ni ad-atoms surface transport properties at different growth rates during the formation of 1 μm thickness Ni films: (a) $J = 10\ \text{mA cm}^{-2}$ and (b) $J = 22\ \text{mA cm}^{-2}$.

of values previously obtained with Ni–Zn alloy electrodeposits on Cu substrate [7]. One is away from the values $10^{-5}$ to $10^{-7}\ \text{cm}^2\ \text{s}^{-1}$ of ions species in electrolytes [27,28] and $10^{-16}$ to $10^{-13}\ \text{cm}^2\ \text{s}^{-1}$ obtained for Au and Pt electrodeposits grown on polycrystalline substrates of the same materials. Note that estimated values of $10^{-20}$ to $10^{-16}\ \text{cm}^2\ \text{s}^{-1}$ were also reported for the deposition of these materials in vacuum [29]. It should be mentioned that the ITO resistivity is likely to play a determining role in the transport properties of the Ni ad-atoms. Therefore, the $D_s$ values here obtained can be considered as being relative as this substrate material is commercially proposed in a wide range of resistivity values.

The bi-modal feature of the film surface morphology denotes that the Ni ad-atoms preferentially grow in the vertical direction at the particular sites of the nano-crystallites formation. The material transport properties in that vertical direction can be evaluated only from the change in the nano-crystallites size while the horizontal motion can be depicted by the diffusion length ($\Lambda_s$) calculated from Eq. (7). Referring to the mean height of the nano-crystallites

**Table 3**
Dependence of the transport properties on the applied current density in the formation of Ni films having a constant thickness $d = 1$ μm.

| Current density $J$ (mA cm$^{-2}$) | Slope constant of Eq. (4): $B$ | Diffusion coefficient $D_s$ (cm$^2$ s$^{-1}$) | Diffusion length $\Lambda_s$ (nm) |
|---|---|---|---|
| 10 | 1.08 | $1.19 \times 10^{-9}$ | 26.74 |
| 14 | 1.40 | $1.54 \times 10^{-9}$ | 30.45 |
| 18 | 0.63 | $6.93 \times 10^{-10}$ | 20.39 |
| 22 | 0.31 | $3.41 \times 10^{-10}$ | 14.30 |

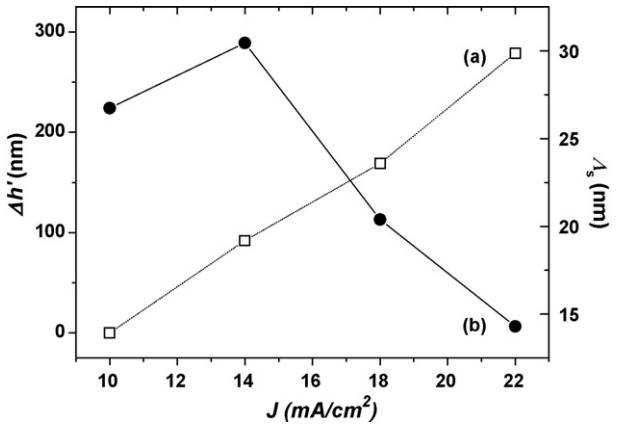


**Fig. 7.** Dependence of the material transport properties of Ni electrodeposits in the two main growth directions: (a) evolution in the vertical direction ($\Delta h'$) and (b) evolution in the horizontal direction ($\Lambda_s$).

obtained at $J = 10\,\mathrm{mA\,cm^{-2}}$ their change in size evaluated by $\Delta h' = (h' - h'_{10})$ is compared to the one of $\Lambda_s$. The study of the current density effect on both parameters clearly shows in Fig. 7 a continuous and monotonic increase of the vertical length while the horizontal one starts with a decreasing trend from $14\,\mathrm{mA\,cm^{-2}}$. This implies that the columnar shape of the nano-crystallites prevails along the range of the investigated $J$ values.

## 4. Conclusion

Because of its transparency and highly conductive characteristic, ITO substrate has been mostly used till now for the deposition of semi-conducting thin films. The growth of metals and particularly nickel thin films on that material has been rarely experimented. We here showed that separated and highly vertical nickel crystallites can be formed on that substrate using the low cost electrodeposition process. The topography study of the resulting nano-structured films confirms the occurrence of a bi-modal morphology feature that appears to be sensitive to the applied current density. The vertical growth is predominant at the particular substrate positions of the crystallites while the horizontal one is favoured in the regions between them. The approach to the surface transport properties including the topography parameter is relevant here as the required condition of linearity between the reciprocal global roughness and the time coefficient has been established. The evaluation of the transport properties in both directions revealed that the increase of the crystallites size occurs with the decrease of the lateral surface diffusion length, which implies that the deposition conditions used with ITO substrate mostly favoured the vertical growth feature. It has been shown by acousto-gyration method that the deposition of gold particles on ITO substrate occurs with different deformation forces [30]. Probably, this kind of forces may also contribute in the formation of the Ni nano-crystallites obtained here. The present work can be considered as preliminary with the final objective of cheaply manufacturing more isolated and bigger nano-crystallites. This is being examined in our team bearing in mind that the size of the small grains in the supporting nano-structured films should be minimised while increasing the one of crystallites. The results proposed here seems encouraging for working furthermore in that direction.

## References

[1] Lorenzo Pavesi, Mater. Today 6 (2005) 18.
[2] C. Thelander, P. Agarwal, S. Brougersma, J. Eymery, L.F. Feiner, A. Forchel, M. Scheffler, W. Reiss, B.J. Ohlsson, U. Gosele, L. Samuelson, Mater. Today 9 (2006) 28.
[3] M. Arruebo, R. Fernandez-Pacheco, M. Ricardo Ibarra, J. Santamaria, Nanotoday 2 (2007) 22.
[4] L. Nzoghe-Mendome, J. Ebothé, A. Aloufy, I. Kityk, J. Alloys Compd. 459 (2008) 232.
[5] W. Schwarzacher, J. Phys. Condens. Matter 16 (2004) R859.
[6] C. Alonso, R.C. Salvarezza, J.M. Varo, A.J. Arvia, L. Vàsquez, A. Bartolomé, A.M. Baro, J. Electrochem. Soc. 137 (1990) 2161.
[7] M. Hiane, J. Ebothé, Eur. Phys. J. B 22 (2001) 485.
[8] K. Lohrberg, P. Kohl, Electrochim. Acta 29 (1984) 2557.
[9] E. Endoh, H. Otouma, T. Morimoto, Y. Oda, Int. J. Hydrogen Energy 12 (1987) 473.
[10] Y. Ni, X. Ge, Z. Zhang, Q. Ye, Chem. Mater. 14 (2002) 1048.
[11] M. Saitou, A. Makabe, T. Tomoyose, Surf. Sci. 459 (2000) L462.
[12] M. Saitou, W. Oshikawa, A. Makabe, J. Phys. Chem. Solids 63 (2002) 1685.
[13] E. Gomez, R. Pollina, E. Vallés, J. Electroanal. Chem. 386 (1995) 45.
[14] J.-L. Pouchou, Anal. Chem. Acta 283 (1993) 81.
[15] H. Benhayoune, N. Dumelié, G. Balossier, Thin Solid Films 493 (2005) 113.
[16] I.V. Kityk, J. Ebothé, G. Chang, M. Oyama, Philos. Mag. Lett. 85 (2005) 549.
[17] F. Family, T. Vicsek, J. Phys. A 18 (1985) L75.
[18] J. Ebothé, A. El Hichou, P. Vautrot, M. Addou, J. Appl. Phys. 93 (2003) 632.
[19] S. Mendez, G. Andreasen, P. Schilardi, M. Figueroa, L. Vàsquez, R.C. Salvarezza, A.J. Arvia, Langmuir 14 (1998) 2515.
[20] J. Ebothé, S. Vilain, J. Phys. D: Appl. Phys. 32 (1999) 2342.
[21] A.L. Barabasi, H.E. Stanley, Fractal Concepts in Surface Growth, Cambridge University Press, England, 1995.
[22] I. Otsuka, T. Iwasaki, J. Vac. Sci. Technol. B 14 (1996) 1153.
[23] S. Singh, S. Basu, Surf. Sci. Technol. 201 (2006) 952.
[24] T.J. Oliviera, F.D.A. Aarao Reis, J. Appl. Phys. 101 (2007) 063507.
[25] R.L. Schwoebel, J. Appl. Phys. 40 (1968) 614.
[26] L. Nzoghe-Mendome, Ph.D. Thesis, Université de Reims Champagne Ardenne, France, 2007.
[27] Modern Electrochemistry, 1 edited by J. O'M Bockris, A.K.N. Reddy, Plenum/Rosetta, New York, 1977.
[28] Z. Petrovic, M. Metikos-Hukovic, Z. Grubac, S. Omanovic, Thin Solid Films 513 (2006) 193.
[29] J. Schewers, R. Sonnenfeld, O. Marti, P.K. Hansma, J.E. Demuth, J. Harmers, J. Appl. Phys. 63 (1988) 717.
[30] I.V. Kityk, A. Umar, M. Oyama, Appl. Opt. 44 (2005) 6905.